

Quantification of Oscillatory Shear Stress from Reciprocating CSF Motion on 4D Flow Imaging

 S. Yamada,  H. Ito,  M. Ishikawa,  K. Yamamoto,  M. Yamaguchi,  M. Oshima, and  K. Nozaki



ABSTRACT

BACKGROUND AND PURPOSE: Oscillatory shear stress could not be directly measured in consideration of direction, although cerebrospinal fluid has repetitive movements synchronized with heartbeat. Our aim was to evaluate the importance of oscillatory shear stress in the cerebral aqueduct and foramen magnum in idiopathic normal pressure hydrocephalus by comparing it with wall shear stress and the oscillatory shear index in patients with idiopathic normal pressure hydrocephalus.

MATERIALS AND METHODS: By means of the 4D flow application, oscillatory shear stress, wall shear stress, and the oscillatory shear index were measured in 41 patients with idiopathic normal pressure hydrocephalus, 23 with co-occurrence of idiopathic normal pressure hydrocephalus and Alzheimer-type dementia, and 9 age-matched controls. These shear stress parameters at the cerebral aqueduct were compared with apertures and stroke volumes at the foramen of Magendie and cerebral aqueduct.

RESULTS: Two wall shear stress magnitude peaks during a heartbeat were changed to periodic oscillation by converting oscillatory shear stress. The mean oscillatory shear stress amplitude and time-averaged wall shear stress values at the dorsal and ventral regions of the cerebral aqueduct in the idiopathic normal pressure hydrocephalus groups were significantly higher than those in controls. Furthermore, those at the ventral region of the cerebral aqueduct in the idiopathic normal pressure hydrocephalus group were also significantly higher than those in the co-occurrence of idiopathic normal pressure hydrocephalus with Alzheimer-type dementia group. The oscillatory shear stress amplitude at the dorsal region of the cerebral aqueduct was significantly associated with foramen of Magendie diameters, whereas it was strongly associated with the stroke volume at the upper end of the cerebral aqueduct rather than that at the foramen of Magendie.

CONCLUSIONS: Oscillatory shear stress, which reflects wall shear stress vector changes better than the conventional wall shear stress magnitude and the oscillatory shear index, can be directly measured on 4D flow MR imaging. Oscillatory shear stress at the cerebral aqueduct was considerably higher in patients with idiopathic normal pressure hydrocephalus.

ABBREVIATIONS: AD = Alzheimer-type dementia; iNPH = idiopathic normal pressure hydrocephalus; OSI = oscillatory shear index; OSS = oscillatory shear stress; TAWSS = time-averaged wall shear stress; WSS = wall shear stress

Impaired CSF absorption might be caused by increased CSF volume in idiopathic normal pressure hydrocephalus (iNPH); however, its etiology has not been elucidated. Stroke volume at the cerebral aqueduct has been reported to be considerably increased in most patients with iNPH.¹⁻⁹ Our previous study on 4D flow MR

imaging revealed that patients with iNPH had significantly increased reciprocating bidirectional CSF movements and flow-related bimodal high wall shear stress (WSS), a force vector produced by the fluid flow acting tangentially on the wall surfaces at the cerebral aqueduct in 1 cardiac cycle.¹⁰ Moreover, high time-averaged wall shear stress (TAWSS) due to bidirectional CSF movements at the cerebral aqueduct was significantly associated with z-axis expansion of the frontal horn of the lateral ventricles in iNPH. WSS is known to regulate vessel caliber and influences the development of vascular pathologies.¹¹⁻²⁰ Oscillating flow dynamics, specifically turbulent or disturbed flow, has been noticed


Received May 22, 2020; accepted after revision October 5.

From the Department of Neurosurgery (S.Y., K.N.), Shiga University of Medical Science, Shiga, Japan; Department of Neurosurgery and Normal Pressure Hydrocephalus Center (S.Y., K.Y., M.Y.), Rakuwakai Otowa Hospital, Kyoto, Japan; Interfaculty Initiative in Information Studies/Institute of Industrial Science (S.Y., M.O.), The University of Tokyo, Tokyo, Japan; Medical System Research and Development Center (H.I.), Fujifilm Corporation, Tokyo, Japan; and Rakuwa Villa Ilios (M.I.), Kyoto, Japan.

The funding sources for the study had no role in the design and conduct of the study; in the collection, analysis, and interpretation of the data; or in the preparation, review, or approval of the manuscript.

This research received grants from the G-7 Scholarship Foundation for 1 year in 2020, the Taiju Life Social Welfare Foundation for 1 year in 2020, and the Fujifilm Corporation for 2 years since 2019.

Please address correspondence to Shigeki Yamada, MD, PhD, Department of Neurosurgery, Shiga University of Medical Science, Seta Tsukinowa-cho, Otsu, Shiga, 520-2192, Japan; e-mail: shigekiyamada39@gmail.com

 Indicates article with online supplemental data.

<http://dx.doi.org/10.3174/ajnr.A6941>

in the pathogenesis of flow-mediated arterial dilation or atherosclerosis.¹¹⁻²⁰ Oscillating low WSS due to turbulent flow at the arterial bifurcation is associated with atherosclerotic plaque,^{11,16-18} whereas chronic high WSS contributes to expansive or outward remodeling of vessels in response to a sustained increase in flow.^{19,20}

In the CSF dynamics, the normal CSF movements generated by the directional beating of motile cilia on the ependymal cells lining the ventricular surface maintain a calm environment in the ventricles; however, increased reciprocating bidirectional CSF movements might induce the disruption of motile cilia and ependymal gliosis, which has been shown to be directly associated with ventriculomegaly.²¹⁻²⁶ Therefore, we hypothesized whether oscillatory shear stress (OSS) due to bidirectional CSF movements at the cerebral aqueduct may also be associated with the size of the cerebral aqueduct and ventricles in iNPH. However, OSS could not be directly measured, which was different from the conventional WSS magnitude without direction information or the oscillatory shear index (OSI), indicating direction changes. Therefore, a novel method to directly measure OSS using 4D flow MR imaging was successfully developed. This study aimed to evaluate the significance of OSS at the cerebral aqueduct and foramen of Magendie in iNPH by comparing it with the conventional WSS magnitude and OSI. Furthermore, shear stress parameters were compared with apertures and stroke volumes at the foramen of Magendie and cerebral aqueduct among patients with iNPH only, patients with co-occurrence of iNPH and Alzheimer-type dementia (AD), and age-matched controls.

MATERIALS AND METHODS

The ethics committees for human research of Rakuwakai Otowa Hospital approved the study design and protocol (Nos. Rakuoto-Rin-17-041 and R2019-227). After obtaining written informed consent from patients or their relatives, the private information was anonymized in a linkable manner. Data collection, anonymization, image acquisition, and data-processing methods of 4D flow MR imaging were described in our previous study.¹⁰ In brief, 64 patients diagnosed with iNPH and 9 age-matched controls who underwent MR imaging examinations from January 28, 2017, to August 30, 2019, using a 3T MR imaging system (Magnetom Skyra; Siemens) were included in this study. All patients with iNPH had gait disturbance, cognitive impairment, and/or urinary incontinence, which improved after the CSF tap test, and ventricular dilation, an enlarged Sylvian fissure, and narrow sulci at the high convexity on conventional CT or MR imaging. A total of 23 patients with iNPH also had clinical AD based on the comprehensive assessment of their symptoms and findings on MR imaging and SPECT. Furthermore, 9 participants 60 years of age or older were recruited as controls because they had no symptoms of a short-stepped gait and/or cognitive impairment.

The time-resolved 3D velocity-encoding data were obtained from the 4D flow MR imaging sequence with 5 cm/s of velocity encoding and synchronizing the peripheral pulse rate measured from the finger (TR, 100 ms; TE, 9 ms; flip angle, 8°; FOV, 200 mm; matrix, 192 × 192; and voxel size, 1.0 × 1.0 × 1.3 mm). The image range was obtained in the midsagittal plane with a width of 30 mm (1.26 mm × 24 slices) from the bilateral foramina

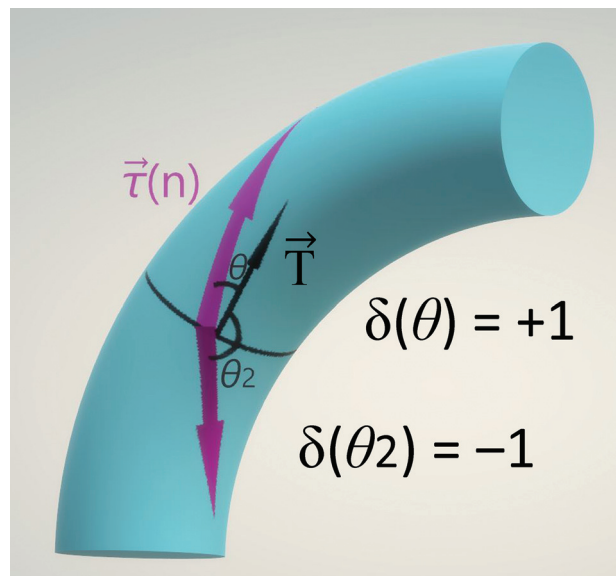


FIG 1. Schema explaining OSS: $\theta(n)$ is the angle between \vec{T} and $\vec{\tau}(n)$ in the n th phase $\vec{\tau}(n)$

$$\delta[\theta(n)] : \begin{cases} +1(-90^\circ < \theta(n) < 90^\circ) \\ -1(90^\circ < \theta(n) < 270^\circ) \end{cases},$$

Where $\vec{T} : \sum_{n=1}^N \vec{\tau}(n)$ indicates a vector of TAWSS, and $\vec{\tau}(n) : \mu \frac{\Delta \vec{v}(n)}{\Delta z}$ indicates a vector of WSS.

of Monro to the upper cervical subarachnoid spaces. All 4D flow analyses were conducted using the 4D flow application in an independent 3D volume analyzer workstation (Synapse 3D; Fujifilm Healthcare). To increase the accuracy of fine anatomic information of <1 mm, we used volumetric data on a T2-weighted 3D spin-echo sequence with sampling perfection with application-optimized contrasts by using different flip angle evolution (SPACE sequence; Siemens). Sequence parameters (TR, 2800 ms; TE, 286 ms; FOV, 230 mm; matrix, 192 × 192; and voxel size, 0.6 × 0.6 × 0.9 mm) were superimposed on 3D phase images using a trilinear interpolation algorithm, and a 3D polygon mesh of ventricles and subarachnoid spaces was created from this high-resolution volumetric data using a marching cubes algorithm (Online Supplemental Data). In all 4D flow analyses, stress parameters were measured after confirming the absence of phase aliasing or motion artifacts. The anterior-posterior diameters of the foramen of Magendie, the lower and upper ends of the cerebral aqueduct, and the mid-brain were measured on the midsagittal plane of T2-weighted 3D SPACE MR imaging (Online Supplemental Data).

The 3D flow velocities (centimeters/second) and volumes (milliliters/second) of the reciprocating CSF movements through 12 ROIs were measured from the bilateral foramina of Monro to the lower end of the second cervical vertebra. The stroke volume was calculated by adding the absolute forward and backward CSF flow volumes, and reversed flow rate (%) by the absolute backward flow volume divided by the absolute forward flow volume. The surface mesh of CSF spaces was generated by increasing the image resolution and applying maximum smoothing, with an

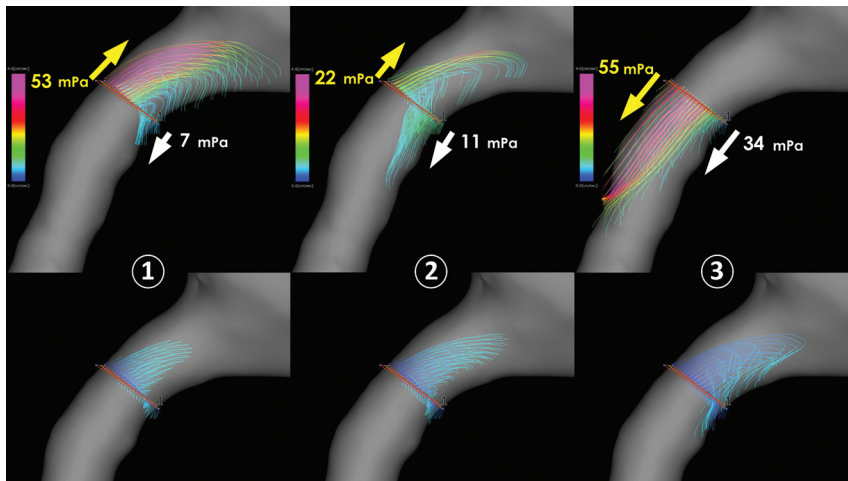


FIG 2. Oscillation of WSS due to bidirectional CSF flow through the cerebral aqueduct. The numbers 1, 2, and 3 demonstrate temporal changes of the reciprocating CSF motion during 1 cardiac cycle in a 77-year-old man diagnosed with iNPH. The colored path lines (lower figures) show the flow as a moving trajectory of the virtual particle through the middle part of the cerebral aqueduct in 1 heartbeat. The color and length of 3D streamlines (upper figures) indicate the flow velocity as pink for fast and blue for slow. The sampling interval of streamlines and path lines was set at 0.2 mm after the trilinear interpolation. The arrows indicate the WSS vector produced by the flow parallel to the wall surface. The size and direction of the arrows indicate the magnitude and direction of the WSS vector. Temporal changes of the WSS vector at the dorsal region (yellow arrows) were larger than those at the ventral region (white arrows).

interpolation of a one-fourth interval and a decimation rate of 50%.

Shear Stress Parameters

The conventional WSS vector in the n th phase $\vec{\tau}(n)$ (N/m^2) was calculated as

$$\vec{\tau}(n) = \mu \frac{\Delta \vec{v}(n)}{\Delta z},$$

where Δz was the distance perpendicular to the wall, $\Delta \vec{v}(n)$ was the flow velocity vector in the n th phase parallel to the wall separate from Δz , and μ was the dynamic viscosity. In this study, Δz was set at 0.8 mm considering the resolution and average diameter of the cerebral aqueduct, and μ was set 1.0×0.001 (pascal \times second) based on the CSF modeled as an incompressible Newtonian fluid with hydrodynamic characteristics of water.

The WSS magnitude $|\vec{\tau}(n)|$ was defined as an absolute value without direction information.

To evaluate the cumulative effect of WSS vector during 1 heartbeat, we calculated the TAWSS vector \vec{T} as

$$\vec{T} = \frac{\sum_{n=1}^N \vec{\tau}(n)}{N},$$

where N was the total number of phases during 1 cardiac cycle and TAWSS magnitude $|\vec{T}|$ was defined as a scalar quantity of the TAWSS vector.

The angle between the n th phase direction of the WSS vector and the TAWSS vector as the principal axis was defined as $\theta(n)$,

and the scale for converting $\theta(n)$ into a binary value of +1 or -1 was defined as $\delta[\theta(n)]$, calculated as

$$\delta[\theta(n)] = \begin{cases} +1 & (-90^\circ < \theta(n) < 90^\circ) \\ -1 & (90^\circ < \theta(n) < 270^\circ) \end{cases},$$

where $\delta(\theta) = +1$ indicates the same direction as \vec{T} and $\delta(\theta) = -1$ indicates a 180° opposite direction. As shown in Fig 1, the WSS magnitude multiplied by +1 or -1 was defined as OSS calculated as

$$\text{OSS} = |\vec{\tau}(n)| \times \delta[\theta(n)].$$

The OSS amplitude was calculated as the maximum minus the minimum OSS value.

OSI that monitors the direction changes of the WSS vector during 1 cardiac cycle was calculated as

$$\text{OSI} = \frac{1}{2} \left\{ 1 - \frac{\left| \sum_{n=1}^N \vec{\tau}(n) \right|}{\sum_{n=1}^N |\vec{\tau}(n)|} \right\}.$$

The OSI ranges from 0 to 0.5, where 0 indicates a complete unidirectional flow and 0.5 indicates oscillatory flow only.

The WSS magnitude and OSI were automatically calculated per pixel and displayed on the 3D surface display using a scalable color map of the 4D flow application on Synapse 3D.

Data and codes used in this study are not available within the public domain because of the commercially available workstation.

The WSS magnitude, OSS, and OSI were automatically measured using 5 dotlike ROIs with the highest WSS magnitude at the ventral (ROI 1) and dorsal (ROI 2) regions of the foramen magnum and dorsal (ROI 3) and ventral (ROI 4) regions of the cerebral aqueduct and interpeduncular cistern (ROI 5).

Statistical Analysis

The Kruskal-Wallis rank sum test was used to compare the mean values [SD] for age and several MR imaging measurements among the 3 groups. In addition, the Wilcoxon rank sum test was used to compare continuous variables between patients with iNPH with co-occurrence of iNPH and AD or controls. The Fisher exact test was used to compare the 3 proportions. The Pearson correlation coefficient (r) and 95% CI were used to determine relationships between shear stress and morphologic parameters or stroke volume. Statistical significance was assumed at a P value $< .05$. All missing data points were treated as deficit data that did not affect other variables. Statistical analyses were performed using R statistical and computing software (Version 3.6.2; <http://www.R-project.org>).

RESULTS

During 1 cardiac cycle, the CSF moved in the craniocaudal and caudocranial directions periodically through the cerebral

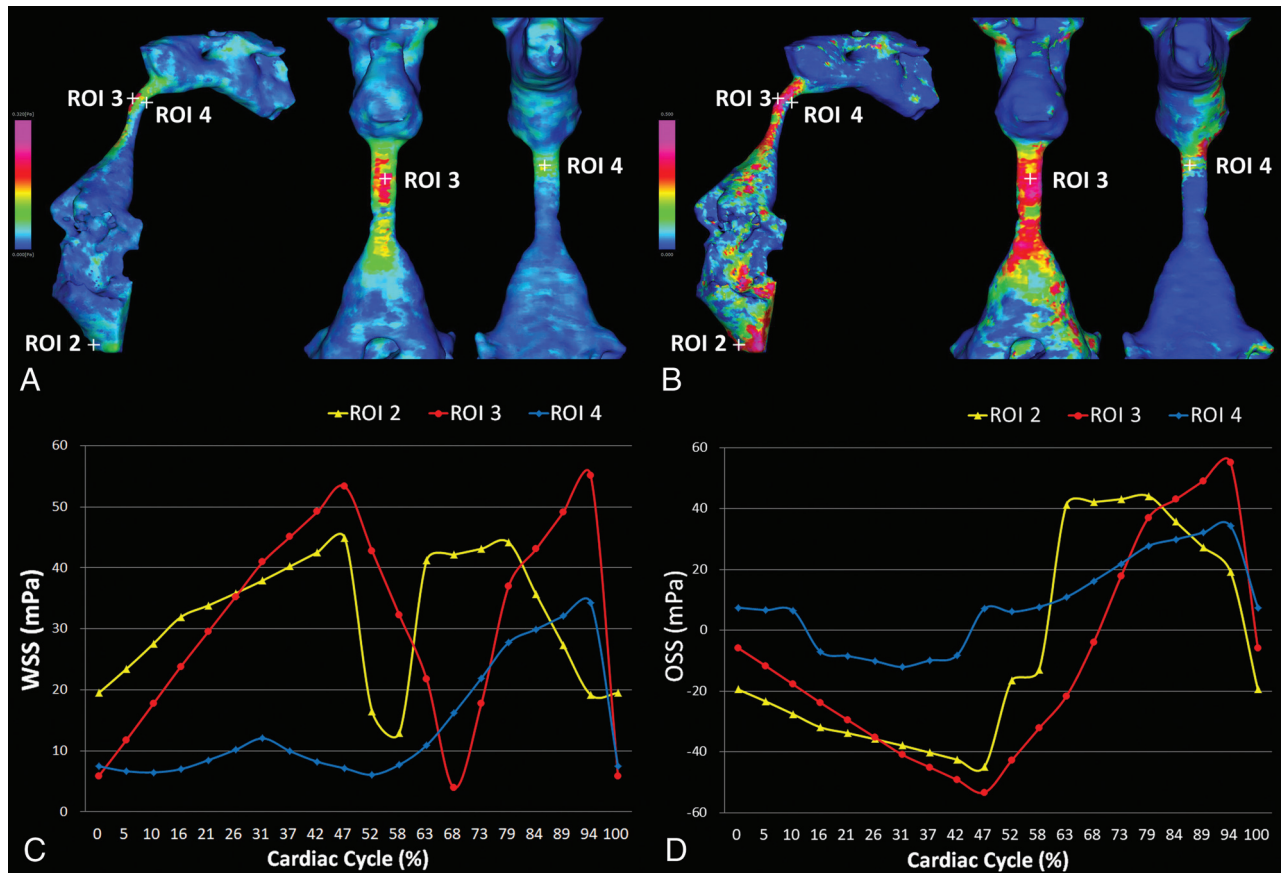


FIG 3. Distributions and fluctuations of shear stress parameters per heartbeat in iNPH. The colored surfaces in the ventricles show the distribution of WSS magnitude (A) and OSI (B) in the same patient with iNPH, as shown in Fig 2. Red indicates high and blue indicates low. Line-graphs C and D show chronologic changes of WSS magnitude and OSS at the dorsal region of the foramen magnum (ROI 2, yellow) and dorsal (ROI 3, red) and ventral (ROI 4, blue) regions of the cerebral aqueduct in 1 cardiac cycle. Considering the shear stress direction, these changes were completely different.

Table 1: Clinical and morphologic characteristics of the study population^a

	iNPH Only	iNPH with AD	Control	P Value
Total number	41	23	9	
Male/female	28:13	13:10	4:5	.332
Age (yr)	78.2 [SD, 6.62]	79.8 [SD, 5.83]	75.7 [SD, 5.70]	.207
Anteroposterior diameter (mm)				
Foramen of Magendie	5.72 [SD, 1.77]	5.88 [SD, 2.04]	2.02 [SD, 0.44]	<.001
Lower end of cerebral aqueduct	4.44 [SD, 0.87]	4.25 [SD, 1.41]	2.23 [SD, 0.70]	<.001
Upper end of cerebral aqueduct	3.65 [SD, 0.66]	3.45 [SD, 0.73]	2.30 [SD, 0.54]	<.001
Midbrain	8.56 [SD, 0.88]	8.43 [SD, 0.92]	9.32 [SD, 1.57]	.230
Stroke volume (μ L/heartbeat)				
Foramen of Magendie	32.9 [SD, 22.6]	37.4 [SD, 37.6]	21.1 [SD, 11.7]	.448
Lower end of cerebral aqueduct	37.6 [SD, 28.9]	39.6 [SD, 43.7]	17.8 [SD, 13.0]	.083
Upper end of cerebral aqueduct	49.0 [SD, 33.3]	52.6 [SD, 32.5]	18.9 [SD, 10.5]	.002
Foramina of Monro	96.5 [SD, 41.0]	97.8 [SD, 39.1]	62.8 [SD, 44.6]	.042

^aData are means. P value is from the Kruskal-Wallis rank sum test.

aqueduct (Fig 2 and Online Supplemental Data). Bidirectional CSF movements at the dorsal region of the cerebral aqueduct were larger than those in the ventral region in patients with iNPH. Chronologic WSS magnitude changes in the dorsal region of the cerebral aqueduct were also larger than those in the ventral region due to bidirectional CSF movements (Fig 3 and Online

Supplemental Data). The distribution of WSS magnitude (Fig 3A) was somewhat different from that of the OSI (Fig 3B). The bimodal high WSS magnitude in Fig 3C at the dorsal region of the foramen magnum (ROI 2) and cerebral aqueduct (ROI 3) was changed to the periodic oscillation by converting OSS (Fig 3D). In other words, 1 of the 2 WSS magnitude peaks during a heartbeat was converted to the negative OSS.

A total of 73 participants comprising 41 patients diagnosed with iNPH only, 23 with co-occurrence of iNPH and AD,

and 9 age-matched controls were included in this study (Table 1).

The difference in mean OSS amplitude, TAWSS, and OSI at the ventral (ROI 1) and dorsal (ROI 2) regions of the foramen magnum and interpeduncular cistern (ROI 5) was not significant among the 3 groups. Therefore, the amplitude, maximum, and

Table 2: Mean value [SD] of parameters at the cerebral aqueduct in the study population^a

	All (n = 73)	iNPH Only (n = 41)	iNPH with AD (n = 23)	Control (n = 9)	P1	P2	P3
Dorsal region of the cerebral aqueduct							
OSS amplitude	52.5 [SD, 33.9]	59.7 [SD, 34.1]	52.9 [SD, 32.2]	19.8 [SD, 13.3]	.483	<.001	.004
Maximum OSS	35.9 [SD, 16.0]	38.7 [SD, 15.5]	37.3 [SD, 16.1]	19.7 [SD, 6.3]	.566	<.001	.002
Minimum OSS	-16.7 [SD, 19.8]	-21.0 [SD, 20.2]	-15.6 [SD, 18.9]	-0.1 [SD, 9.6]	.277	.001	.043
TAWSS	18.2 [SD, 8.9]	19.7 [SD, 8.7]	18.8 [SD, 9.3]	9.9 [SD, 2.2]	.678	<.001	.008
OSI	0.21 [SD, 0.13]	0.24 [SD, 0.12]	0.19 [SD, 0.14]	0.16 [SD, 0.11]	.234	.077	.614
Ventral region of the cerebral aqueduct							
OSS amplitude	27.2 [SD, 28.4]	36.0 [SD, 32.2]	18.1 [SD, 19.8]	11.9 [SD, 11.1]	.022	.020	.363
Maximum OSS	23.6 [SD, 15.9]	28.8 [SD, 17.9]	18.2 [SD, 10.9]	14.2 [SD, 6.4]	.017	.011	.246
Minimum OSS	-3.6 [SD, 13.9]	-7.1 [SD, 15.9]	0.14 [SD, 10.1]	2.3 [SD, 7.5]	.080	.091	.592
TAWSS	12.2 [SD, 7.1]	14.3 [SD, 8.1]	10.1 [SD, 4.9]	8.1 [SD, 2.7]	.038	.020	.458
OSI	0.13 [SD, 0.15]	0.15 [SD, 0.15]	0.10 [SD, 0.14]	0.11 [SD, 0.15]	.114	.355	.910

^a P1 indicates probability value of iNPH only versus iNPH with AD by the Wilcoxon rank sum test; P2, probability value of iNPH only versus controls by the Wilcoxon rank sum test; and P3, probability value of iNPH with AD versus controls by the Wilcoxon rank sum test.

minimum OSS values; TAWSS; and OSI at the dorsal (ROI 3) and ventral (ROI 4) regions of the cerebral aqueduct are shown in Table 2. The mean OSS amplitude at the dorsal and ventral regions of the cerebral aqueduct in the iNPH groups was approximately 3 times higher than that in the controls because the maximum OSS in the iNPH groups was twice as high and the minimum OSS was considerably lower. Remarkably, the mean amplitude and maximum OSS values at the ventral region of the cerebral aqueduct in the iNPH-only group were twice as high as those in the iNPH with AD group. The mean TAWSS magnitude at the dorsal region of the cerebral aqueduct in the iNPH-only group was also significantly higher than that in the controls. Furthermore, patients with iNPH-only had a significantly higher mean TAWSS magnitude at the ventral region of the cerebral aqueduct compared with those with iNPH with AD. The median and distribution of the OSS amplitude and TAWSS magnitude at the dorsal and ventral regions of the cerebral aqueduct among the 3 groups are shown as boxplots in Fig 4. Both the OSS amplitude and TAWSS magnitude at the dorsal region of the cerebral aqueduct in the iNPH groups were significantly higher than those in the controls, whereas the OSS amplitude at the ventral region of the cerebral aqueduct in the iNPH-only group was significantly higher than that in the iNPH with AD group and controls. The difference in OSI was not significant among the 3 groups.

The TAWSS magnitude was strongly associated with the amplitude and maximum and minimum OSS values at the dorsal ($r = 0.89, 0.93,$ and -0.77) and ventral ($r = 0.88, 0.93,$ and -0.73) regions of the cerebral aqueduct (Online Supplemental Data).

Relationships between Shear Stress Parameters and Anterior-Posterior Diameter or Stroke Volume

The amplitude and maximum and minimum OSS values and TAWSS magnitude at the dorsal region of the cerebral aqueduct were significantly associated with the anterior-posterior diameters of the foramen of Magendie and the lower end of the cerebral aqueduct (Table 3) and were strongly associated with stroke volume at the upper and lower ends of the cerebral aqueduct and foramen of Magendie, respectively (Table 4). The amplitude and maximum and minimum OSS values and TAWSS magnitude at the ventral region of the cerebral aqueduct were significantly-but-weakly

associated with stroke volumes at the lower and upper ends of the cerebral aqueduct. However, OSI was not significantly associated with anterior-posterior diameters or stroke volumes at any locations.

DISCUSSION

The reciprocating bidirectional CSF movements increase the bimodal WSS magnitude at the cerebral aqueduct during a cardiac cycle in iNPH. The conventional WSS magnitude was calculated as an absolute value of the WSS vector without the direction information by converting to a scalar quantity. However, the actual shear stress was produced by the bidirectional CSF flows from positive to negative values, not in a bimodal waveform. Therefore, a novel parameter, OSS with plus/minus directional information in addition to the WSS magnitude, was developed. On the basis of our literature review, this study is the first report that directly measures the OSS on 4D flow MR imaging. The maximum value of positive OSS drastically fluctuated to the minimum value of negative OSS during a heartbeat due to the reciprocating CSF movements in iNPH. Conversely, the maximum WSS magnitude value was either of the 2 peaks, whereas the minimum value was nearly zero consistently. However, the TAWSS magnitude was significantly associated with the OSS amplitude.

The distribution and magnitude of OSI were different from those of OSS or WSS magnitude. In contrast to steady flow conditions, pulsatile bidirectional flows cause large OSS fluctuations.

In this study, the OSS amplitude at the dorsal region of the cerebral aqueduct was significantly associated with both the foramen of Magendie diameters and stroke volumes at the upper and lower ends of the cerebral aqueduct and foramen of Magendie, respectively. Our previous study demonstrated that the stroke volume at the cerebral aqueduct had the strongest association with the foramen of Magendie diameter.¹⁰ These findings indicate that the dilation of the foramen of Magendie may be the first trigger for increased OSS amplitude at the dorsal region of the cerebral aqueduct due to increased aqueductal stroke volume. On the basis of study on oscillating flow dynamics,¹¹⁻²⁰ chronic high OSS at the cerebral aqueduct may be involved in the expansive remodeling of the aqueductal lumen diameter and may

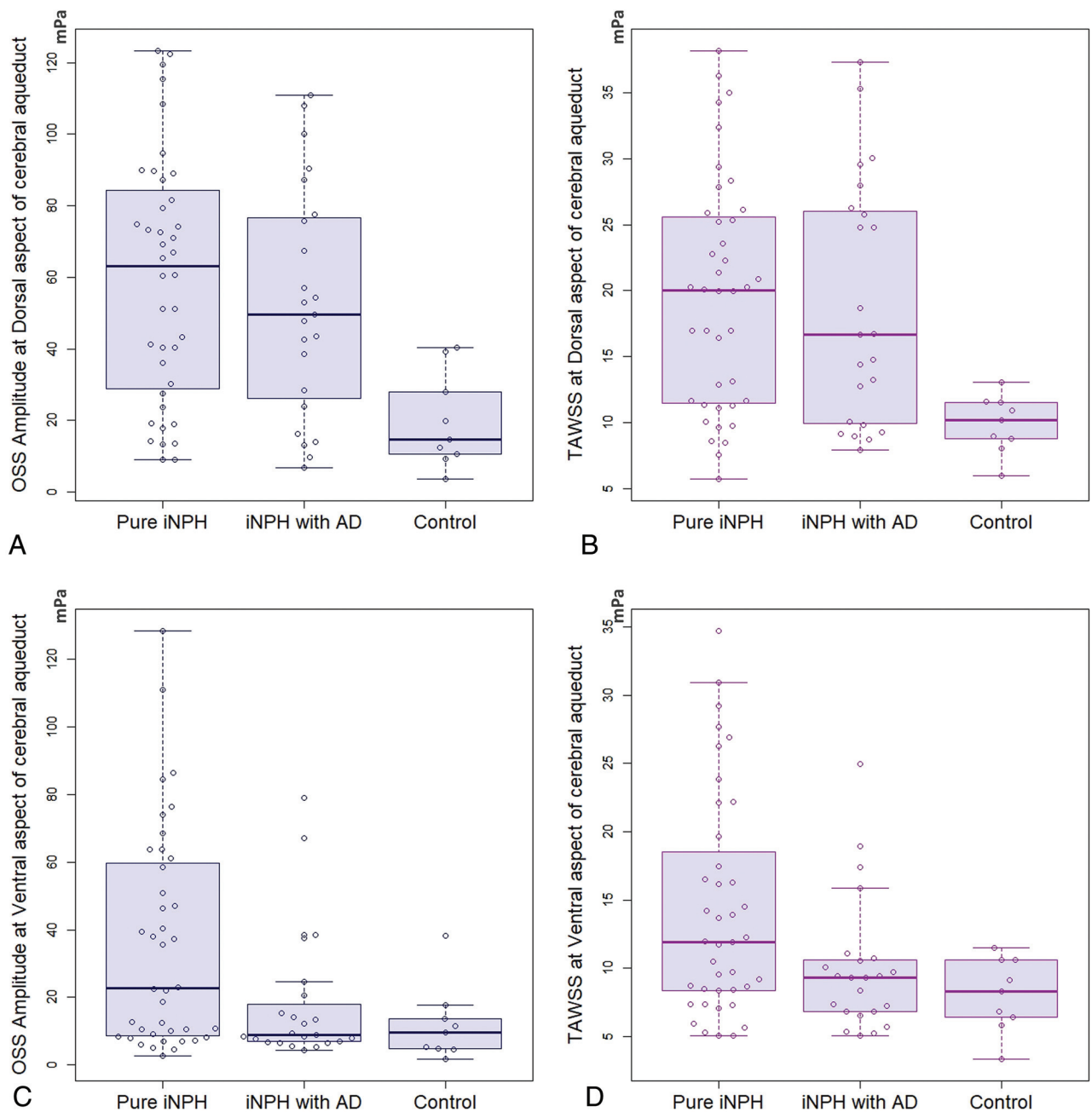


FIG 4. Boxplots for the amplitude of OSS and TAWSS at the dorsal and ventral regions of the cerebral aqueduct among 3 groups. *A*, Distribution of the OSS amplitude at the dorsal region of the cerebral aqueduct. *B*, Distribution of the TAWSS at the dorsal region of the cerebral aqueduct. *C*, Distribution of the OSS amplitude at the ventral region of the cerebral aqueduct. *D*, Distribution of the TAWSS at the ventral region of the cerebral aqueduct.

subsequently increase the pulsatile CSF inflow. However, this study has not yet proved this evidence.

Increased OSS amplitude may be associated with symptoms or pathologies of iNPH. We found that patients with iNPH-only had significantly higher OSS amplitude only at the ventral region of the cerebral aqueduct compared with those with co-occurrence of iNPH and AD. This finding was consistent with our previous result that patients with iNPH-only had not only smaller ventricular volume but also larger basal cistern and Sylvian fissure volumes than those with co-occurrence of iNPH and AD.²⁷ AD is known as the most common comorbidity with iNPH due to CSF stagnation,²⁸⁻³² hindering the clearance of neurotoxic molecules such as amyloid- β or τ .^{33,34} Recently, pulsatile CSF inflow to the ventricular

systems during sleep was reportedly associated with large, coupled low-frequency oscillations in the neuronal activity and hemodynamic oscillations.³⁵ Decreased CSF pulsation may be associated with AD onset through the pathway in suppressed electrophysiologic slow waves that impair amyloid- β and τ excretion into the brain interstitial fluid and CSF during sleep.³⁶⁻³⁹ Therefore, direct OSS measurement in future studies will help determine whether CSF oscillations are associated with the AD onset.

This study had some limitations as described in our previous study.¹⁰ In particular, influences of respiration, wall motion, eddy currents, and background noise on the 4D flow MR imaging sequence were not assessed. Second, OSS and WSS magnitudes calculated by 4D flow MR imaging may be underestimated compared

Table 3: Relationships with anterior-posterior diameter by the Pearson correlation coefficient (95% confidence intervals)

	Foramen of Magendie	Lower End of Cerebral Aqueduct	Upper End of Cerebral Aqueduct	Midbrain
Dorsal region of the cerebral aqueduct				
OSS amplitude	0.55 (0.36–0.69)	0.47 (0.26–0.63)	0.28 (0.05–0.48)	NS
Maximum OSS	0.53 (0.34–0.68)	0.41 (0.20–0.59)	NS	NS
Minimum OSS	–0.51 (–0.66 to –0.31)	–0.46 (–0.63 to –0.26)	–0.32 (–0.51 to –0.10)	NS
TAWSS	0.56 (0.37–0.70)	0.40 (0.18–0.58)	NS	NS
OSI	NS	NS	NS	NS
Ventral region of the cerebral aqueduct				
OSS amplitude	NS	0.27 (0.04–0.47)	NS	NS
Maximum OSS	NS	0.31 (0.08–0.50)	NS	NS
Minimum OSS	NS	NS	NS	NS
TAWSS	0.26 (0.04–0.47)	0.33 (0.10–0.52)	NS	NS
OSI	NS	NS	NS	NS

Note:—NS indicates not significant ($P \geq .05$) by the Pearson correlation analysis.

Table 4: Relationships with stroke volume by the Pearson correlation coefficient (95% confidence intervals)

	Foramen of Magendie	Lower End of Cerebral Aqueduct	Upper End of Cerebral Aqueduct	Foramina of Monro
Dorsal region of the cerebral aqueduct				
OSS amplitude	0.48 (0.28–0.64)	0.53 (0.34–0.68)	0.63 (0.47–0.76)	NS
Maximum OSS	0.50 (0.31–0.66)	0.56 (0.37–0.70)	0.66 (0.50–0.77)	NS
Minimum OSS	–0.41 (–0.59 to –0.20)	–0.46 (–0.63 to –0.26)	–0.55 (–0.70 to –0.37)	NS
TAWSS	0.43 (0.22–0.60)	0.53 (0.34–0.68)	0.73 (0.60–0.82)	NS
OSI	NS	NS	NS	NS
Ventral region of the cerebral aqueduct				
OSS amplitude	NS	0.30 (0.07–0.50)	0.25 (0.02–0.46)	NS
Maximum OSS	NS	0.32 (0.10–0.52)	0.29 (0.07–0.49)	NS
Minimum OSS	NS	–0.24 (–0.45 to –0.01)	NS	NS
TAWSS	NS	0.37 (0.15–0.55)	0.34 (0.12–0.53)	NS
OSI	NS	NS	NS	NS

Note:—NS indicates not significant ($P \geq .05$) by the Pearson correlation analysis.

with the true values, though their distribution is considered reasonably accurate.⁴⁰ Third, the AD comorbidity was not pathologically confirmed through brain biopsy, CSF biomarkers, or amyloid imaging in this study. Finally, we were unable to determine a causal relationship between the dilated cerebral aqueduct and increased OSS amplitude because this study had a cross-sectional design. Therefore, a causal relationship should be investigated in a prospective cohort study or basic research.

CONCLUSIONS

OSS as a novel parameter combining the conventional WSS magnitude with a positive or negative sign indicating the WSS direction can be quantitatively measured at any point on 4D flow MR imaging. Therefore, the OSS amplitude produced by reciprocating bidirectional CSF movements reflects WSS vector changes better than the conventional scalar quantities of the WSS magnitude and OSI. Quantitative OSS measurement may help elucidate the pathophysiologic mechanism of ventricular dilation in iNPH or symptom progression. OSS brings a new perspective to the study of slowly and intricately moving CSF in the complex shapes of the ventricles and the subarachnoid space.

ACKNOWLEDGMENTS

We thank the patients and volunteers for their participation and the radiologists for their cooperation in the study. We

also thank Enago (www.enago.com) for the English language review.

Disclosures: Shigeki Yamada—*RELATED: Grant:* Fujifilm Corporation, *Comments:* This study received funding of 500,000/year \times 2 years from Fujifilm Corporation in Japan. Our institute (Shiga University of Medical Science) has signed a research contract with Fujifilm Corporation for the joint development of 3D workstation applications*; *UNRELATED: Grants/Grants Pending:* G-7 Scholarship Foundation, *Comments:* research grant*; *Payment for Lectures Including Service on Speakers Bureaus:* Fujifilm Medical Systems, Integra Japan, and Daiichi Sankyo, *Comments:* Speakers honoraria. Masatsune Ishikawa—*RELATED: Grant:* Health and Labor Sciences Research Grants for the Research on Intractable Diseases, Ministry of Health, Labor and Welfare, Japan, *Comments:* 2017-Nanci-General-037. Kazuhiko Nozaki—*UNRELATED: Grants/Grants Pending:* Japan Agency for Medical Research and Development, grants from KAKENHI, grant from the Japan Society for the Promotion of Science*; *Payment for Lectures Including Service on Speakers Bureaus:* honoraria from Pfizer Japan, Daiichi Sankyo. *Money paid to the institution.

REFERENCES

- Blitz AM, Shin J, Baledent O, et al. **Does phase-contrast imaging through the cerebral aqueduct predict the outcome of lumbar CSF drainage or shunt surgery in patients with suspected adult hydrocephalus?** *AJNR Am J Neuroradiol* 2018;39:2224–30 [CrossRef Medline](#)
- Bradley WG Jr, Whittemore AR, Kortman KE, et al. **Marked cerebrospinal fluid void: indicator of successful shunt in patients with suspected normal-pressure hydrocephalus.** *Radiology* 1991;178:459–66 [CrossRef Medline](#)

3. Bradley WG Jr, Scalzo D, Queralt J, et al. **Normal-pressure hydrocephalus: evaluation with cerebrospinal fluid flow measurements at MR imaging.** *Radiology* 1996;198:523–29 [CrossRef Medline](#)
4. Bunck AC, Kroger JR, Juttner A, et al. **Magnetic resonance 4D flow characteristics of cerebrospinal fluid at the craniocervical junction and the cervical spinal canal.** *Eur Radiol* 2011;21:1788–96 [CrossRef Medline](#)
5. El Sankari S, Gondry-Jouet C, Fichten A, et al. **Cerebrospinal fluid and blood flow in mild cognitive impairment and Alzheimer's disease: a differential diagnosis from idiopathic normal pressure hydrocephalus.** *Fluids Barriers CNS* 2011;8:12 [CrossRef Medline](#)
6. Gupta S, Soellinger M, Grzybowski DM, et al. **Cerebrospinal fluid dynamics in the human cranial subarachnoid space: an overlooked mediator of cerebral disease, I: computational model.** *J R Soc Interface* 2010;7:1195–1204 [CrossRef Medline](#)
7. Krauss JK, Regel JP, Vach W, et al. **Flow void of cerebrospinal fluid in idiopathic normal pressure hydrocephalus of the elderly: can it predict outcome after shunting?** *Neurosurgery* 1997;40:67–74 [CrossRef Medline](#)
8. Lindstrom EK, Ringstad G, Mardal KA, et al. **Cerebrospinal fluid volumetric net flow rate and direction in idiopathic normal pressure hydrocephalus.** *Neuroimage Clin* 2018;20:731–41 [CrossRef Medline](#)
9. Stoquart-ElSankari S, Baledent O, Gondry-Jouet C, et al. **Aging effects on cerebral blood and cerebrospinal fluid flows.** *J Cereb Blood Flow Metab* 2007;27:1563–72 [CrossRef Medline](#)
10. Yamada S, Ishikawa M, Ito H, et al. **Cerebrospinal fluid dynamics in idiopathic normal pressure hydrocephalus on four-dimensional flow imaging.** *Eur Radiol* 2020;30:4454–65 [CrossRef Medline](#)
11. Caro CG, Fitz-Gerald JM, Schroter RC. **Arterial wall shear and distribution of early atheroma in man.** *Nature* 1969;223:1159–60 [CrossRef Medline](#)
12. Dolan JM, Kolega J, Meng H. **High wall shear stress and spatial gradients in vascular pathology: a review.** *Ann Biomed Eng* 2013;41:1411–27 [CrossRef Medline](#)
13. Gibbons GH, Dzau VJ. **The emerging concept of vascular remodeling.** *N Engl J Med* 1994;330:1431–38 [CrossRef Medline](#)
14. Hahn C, Schwartz MA. **Mechanotransduction in vascular physiology and atherogenesis.** *Nat Rev Mol Cell Biol* 2009;10:53–62 [CrossRef Medline](#)
15. Kouzbari K, Hossan MR, Arrizabalaga JH, et al. **Oscillatory shear potentiates latent TGF-beta1 activation more than steady shear as demonstrated by a novel force generator.** *Sci Rep* 2019;9:6065 [CrossRef Medline](#)
16. Ku DN, Giddens DP, Zarins CK, et al. **Pulsatile flow and atherosclerosis in the human carotid bifurcation: positive correlation between plaque location and low oscillating shear stress.** *Arteriosclerosis* 1985;5:293–302 [CrossRef Medline](#)
17. Malek AM, Alper SL, Izumo S. **Hemodynamic shear stress and its role in atherosclerosis.** *JAMA* 1999;282:2035–42 [CrossRef Medline](#)
18. Meng H, Tutino VM, Xiang J, et al. **High WSS or low WSS? Complex interactions of hemodynamics with intracranial aneurysm initiation, growth, and rupture: toward a unifying hypothesis.** *AJNR Am J Neuroradiol* 2014;35:1254–62 [CrossRef Medline](#)
19. Tremblay JC, Thom SR, Yang M, et al. **Oscillatory shear stress, flow-mediated dilatation, and circulating microparticles at sea level and high altitude.** *Atherosclerosis* 2017;256:115–22 [CrossRef Medline](#)
20. Zarins CK, Zatina MA, Giddens DP, et al. **Shear stress regulation of artery lumen diameter in experimental atherogenesis.** *J Vasc Surg* 1987;5:413–20 [CrossRef Medline](#)
21. Hickman TT, Shuman ME, Johnson TA, et al. **Association between shunt-responsive idiopathic normal pressure hydrocephalus and alcohol.** *J Neurosurg* 2017;127:240–48 [CrossRef Medline](#)
22. Kageyama H, Miyajima M, Ogino I, et al. **Panventriculomegaly with a wide foramen of Magendie and large cisterna magna.** *J Neurosurg* 2016;124:1858–66 [CrossRef Medline](#)
23. Morimoto Y, Yoshida S, Kinoshita A, et al. **Nonsense mutation in CFAP43 causes normal-pressure hydrocephalus with ciliary abnormalities.** *Neurology* 2019;92:e2364–74 [CrossRef Medline](#)
24. Mahuzier A, Shihavuddin A, Fournier C, et al. **Ependymal cilia beating induces an actin network to protect centrioles against shear stress.** *Nat Commun* 2018;9:2279 [CrossRef Medline](#)
25. Omran AJA, Saternos HC, Althobaiti YS, et al. **Alcohol consumption impairs the ependymal cilia motility in the brain ventricles.** *Sci Rep* 2017;7:13652 [CrossRef Medline](#)
26. Shook BA, Lenington JB, Acabchuk RL, et al. **Ventriculomegaly associated with ependymal gliosis and declines in barrier integrity in the aging human and mouse brain.** *Aging Cell* 2014;13:340–50 [CrossRef Medline](#)
27. Yamada S, Ishikawa M, Yamamoto K. **Comparison of CSF distribution between idiopathic normal pressure hydrocephalus and Alzheimer disease.** *AJNR Am J Neuroradiol* 2016;37:1249–55 [CrossRef Medline](#)
28. Cabral D, Beach TG, Vedders L, et al. **Frequency of Alzheimer's disease pathology at autopsy in patients with clinical normal pressure hydrocephalus.** *Alzheimers Dement* 2011;7:509–13 [CrossRef Medline](#)
29. Golomb J, Wisoff J, Miller DC, et al. **Alzheimer's disease comorbidity in normal pressure hydrocephalus: prevalence and shunt response.** *J Neurol Neurosurg Psychiatry* 2000;68:778–81 [CrossRef Medline](#)
30. Malm J, Graff-Radford NR, Ishikawa M, et al. **Influence of comorbidities in idiopathic normal pressure hydrocephalus: research and clinical care—a report of the ISHCSF task force on comorbidities in INPH.** *Fluids Barriers CNS* 2013;10:22 [CrossRef Medline](#)
31. Silverberg GD, Mayo M, Saul T, et al. **Alzheimer's disease, normal-pressure hydrocephalus, and senescent changes in CSF circulatory physiology: a hypothesis.** *Lancet Neurol* 2003;2:506–11 [CrossRef Medline](#)
32. Williams MA, Relkin NR. **Diagnosis and management of idiopathic normal-pressure hydrocephalus.** *Neurol Clin Pract* 2013;3:375–85 [CrossRef Medline](#)
33. Jingami N, Uemura K, Asada-Utsugi M, et al. **Two-point dynamic observation of Alzheimer's disease cerebrospinal fluid biomarkers in idiopathic normal pressure hydrocephalus.** *JAD* 2019;72:271–77 [CrossRef Medline](#)
34. Miyajima M, Nakajima M, Ogino I, et al. **Soluble amyloid precursor protein alpha in the cerebrospinal fluid as a diagnostic and prognostic biomarker for idiopathic normal pressure hydrocephalus.** *Eur J Neurol* 2013;20:236–42 [CrossRef Medline](#)
35. Fultz NE, Bonmassar G, Setsompop K, et al. **Coupled electrophysiological, hemodynamic, and cerebrospinal fluid oscillations in human sleep.** *Science* 2019;366:628–31 [CrossRef Medline](#)
36. Diekelmann S, Born J. **The memory function of sleep.** *Nat Rev Neurosci* 2010;11:114–26 [CrossRef Medline](#)
37. Holth JK, Fritsch SK, Wang C, et al. **The sleep-wake cycle regulates brain interstitial fluid tau in mice and CSF tau in humans.** *Science* 2019;363:880–84 [CrossRef Medline](#)
38. Kang JE, Lim MM, Bateman RJ, et al. **Amyloid-beta dynamics are regulated by orexin and the sleep-wake cycle.** *Science* 2009;326:1005–07 [CrossRef Medline](#)
39. Xie L, Kang H, Xu Q, et al. **Sleep drives metabolite clearance from the adult brain.** *Science* 2013;342:373–77 [CrossRef Medline](#)
40. Szajer J, Ho-Shon K. **A comparison of 4D flow MRI-derived wall shear stress with computational fluid dynamics methods for intracranial aneurysms and carotid bifurcations: a review.** *Magn Reson Imaging* 2018;48:62–69 [CrossRef Medline](#)